Hindawi Publishing Corporation
Journal of Nanomaterials
Volume 2014, Article ID 238291, 5 pages
http://dx.doi.org/10.1155/2014/238291

Hindawi

Research Article

Analysis of the High Conversion Efficiencies β-$FeSi_2$ and $BaSi_2$ n-i-p Thin Film Solar Cells

Jung-Sheng Huang, Kuan-Wei Lee, and Yu-Hsiang Tseng

Department of Electronic Engineering, I-Shou University, Kaohsiung 840, Taiwan

Correspondence should be addressed to Jung-Sheng Huang; jshuang@isu.edu.tw

Received 20 June 2014; Revised 20 September 2014; Accepted 22 September 2014; Published 29 December 2014

Academic Editor: Chien-Jung Huang

Both β-$FeSi_2$ and $BaSi_2$ are silicides and have large absorption coefficients; thus they are very promising Si-based new materials for solar cell applications. In this paper, the dc I-V characteristics of n-Si/i-$\beta FeSi_2$/p-Si and n-Si/i-$BaSi_2$/p-Si thin film solar cells are investigated by solving the charge transport equations with optical generations. The diffusion current densities of free electron and hole are calculated first. Then the drift current density in the depletion regions is obtained. The total current density is the sum of diffusion and drift current densities. The conversion efficiencies are obtained from the calculated I-V curves. The optimum conversion efficiency of n-Si/i-$\beta FeSi_2$/p-Si thin film solar cell is 27.8% and that of n-Si/i-$BaSi_2$/p-Si thin film solar cell is 30.4%, both are larger than that of Si n-i-p solar cell (η is 20.6%). These results are consistent with their absorption spectrum. The calculated conversion efficiency of Si n-i-p solar cell is consistent with the reported researches. Therefore, these calculation results are valid in this work.

1. Introduction

A silicide is a compound that has silicon with more electropositive elements. The metal silicides have been widely investigated for several years because of their potential applications in electronics [1]. Semiconducting beta-phase iron disilicide (β-$FeSi_2$) and orthorhombic barium silicide ($BaSi_2$) are two transition metal silicides and they are very promising Si-based new materials for solar cell applications. It is desirable for solar cell materials to have a large absorption coefficient to yield high conversion efficiencies. β-$FeSi_2$ has a large optical absorption coefficient ($>10^5\ cm^{-1}$ at 1.5 eV) and a direct band gap of ~0.87 eV [2–4]. Lin et al. [5] reported a conversion efficiency of 3.7% for p- (or n-) type β-$FeSi_2$/n- (or p-) type Si solar cell. Gao et al. [6] simulated a p-Si/i-$\beta FeSi_2$/n-Si solar cell structure by using the AMPS-1D software. The conversion efficiency is 24.7%. The orthorhombic barium silicide ($BaSi_2$) also has a large absorption coefficient of over $10^5\ cm^{-1}$ at 1.5 eV [7]. Recent reports on the photoresponse properties of $BaSi_2$ have shown that $BaSi_2$ is a new silicide material suitable for solar cell applications [8, 9].

Therefore, in this paper the conversion efficiencies of n-Si/i-$\beta FeSi_2$/p-Si and n-Si/i-$BaSi_2$/p-Si thin film solar cells are investigated by using self-developed analytical methods. For semiconductor solar cells, the n-i-p structure usually has superior I-V characteristics than the n-p structure. Since the built-in electric field exists in the intrinsic layer, the generated electron-hole pairs in the intrinsic layer are drifted by the electric field and produce larger short-circuit current and open-circuit voltage. In addition, the intrinsic silicide layer does not need doping and its manufacturing is compatible with the well-established Si solar cells. The distributions of minority carrier concentrations in the neutral n-Si and p-Si regions are calculated first. Then the total current density is the sum of diffusion current densities of free electron and hole and the drift current density in the depletion regions. The conversion efficiencies are calculated from the I-V curves of the solar cells with illumination of light. The calculated optimum conversion efficiency of β-$FeSi_2$ n-i-p solar cell is 27.8% and that of $BaSi_2$ p-i-n solar cell is 30.4% and that of Si n-i-p solar cell is 20.6%. Therefore, the conversion efficiencies of β-$FeSi_2$ and $BaSi_2$ n-i-p solar cells are significantly larger than that of the conventional Si n-i-p solar cells. The reported

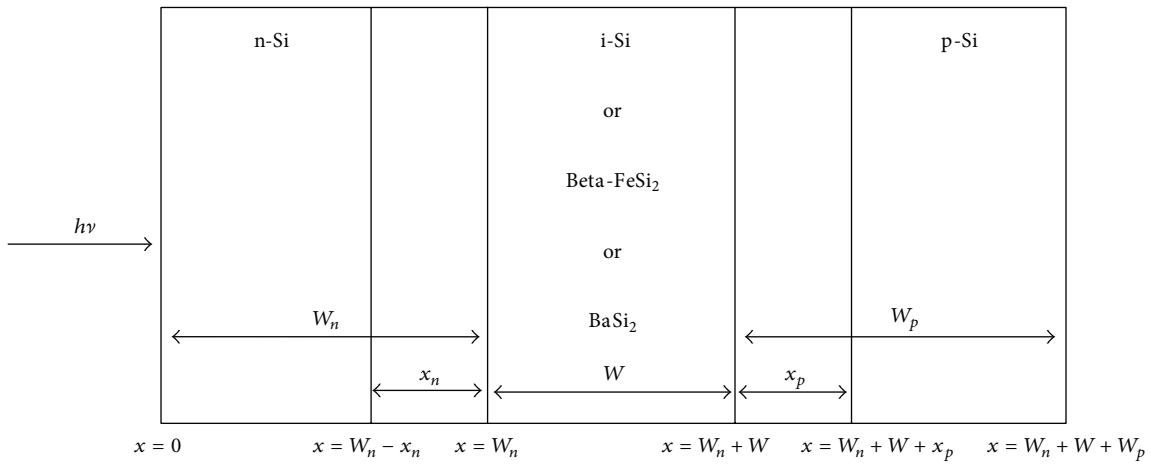

Figure 1: A one-dimensional analysis model of n-i-p thin film solar cells.

conversion efficiency of Si n-i-p solar cell is consistent with this calculation work [10]. Therefore, the calculation results are valid in this work.

2. Analysis Methods

The n-i-p structure of solar cells under investigation is shown in Figure 1. The calculations are under global AM1.5 solar spectrum (Wm^{-2}) at 25°C. At the surface of the solar cell (i.e., at $x = 0$), the generation rate of electron-hole pairs, $G_0(\lambda)$ ($\mathrm{s}^{-1}\mathrm{m}^{-3}$), is [11]

$$G_0(\lambda) = \eta_i [1 - R(\lambda)] \frac{I_{\mathrm{opt}}}{\hbar\omega} \alpha(\lambda), \tag{1}$$

where λ = the wavelength of the incident light (m), η_i = the intrinsic quantum efficiency to account for the average number (100% maximum) of electron-hole pairs generated per incident photon, $R(\lambda)$ = the optical reflectivity between the air and the semiconductor, I_{opt} = the incident optical power intensity (Wm^{-2}), $\hbar\omega$ = the energy of the incident photon (Joul), and $\alpha(\lambda)$ = the absorption spectrum (m^{-1}).

The generation rate of electron-hole pairs in the solar cell device ($x > 0$) is

$$G(x, \lambda) = G_0(\lambda) e^{-\alpha(\lambda)x}. \tag{2}$$

In the neutral n-Si region, the charge transport equation for the excess hole concentration, δP_n, is

$$\frac{d^2}{dx^2}\delta P_n(x, \lambda) - \frac{1}{L_p^2}\delta P_n(x, \lambda) = -\frac{1}{D_p} G(x, \lambda), \tag{3}$$

where L_p = the average diffusion length of holes in n-type region (m) and D_p = the diffusion coefficient of minority holes ($\mathrm{m}^2\mathrm{s}^{-1}$).

The two boundary conditions to solve (3) are as follows.

(a) At the edge of n-Si depletion region ($x = W_n - X_n$):

$$\delta P_n = P_{no}\left[e^{qv/kt} - 1\right]. \tag{4}$$

(b) At the surface of n-Si ($x = 0$):

$$D_p \frac{d}{dx}\delta P_n = S_p \delta P_n, \tag{5}$$

where S_p is the surface recombination velocity of holes (ms^{-1}).

Then the hole diffusion current density is calculated at the edge of the n-Si depletion region as

$$J_{p,\mathrm{diff}} = -qD_p \frac{d}{dx}\delta p_n\Big|_{x=w_n-x_n}. \tag{6}$$

Similarly, the distribution of free electron density, $\delta n_p(x, \lambda)$, in the neutral region of the p-Si can be obtained by solving the charge transport equation for δn_p. And the electron diffusion current density is calculated at the edge of the p-Si depletion region as

$$J_{n,\mathrm{diff}} = qD_n \frac{d}{dx}\delta n_p\Big|_{x=w_n+w+x_p}. \tag{7}$$

The drift current density due to optical generation in the depletion regions is calculated as

$$\begin{aligned} J_{\mathrm{drift}} = {} & q\int_{\text{n-Si}} G_0(\mathrm{Si})\, e^{-\partial(\mathrm{Si})x} dx \\ & + q\int_{\text{i-region}} G_0(\beta - \mathrm{FeSi_2})\, e^{-\partial(\beta-\mathrm{FeSi_2})x} dx \\ & + q\int_{\text{p-Si}} G_0(\mathrm{Si})\, e^{-\partial(\mathrm{Si})x} dx, \end{aligned} \tag{8}$$

where the first term accounts for the drift current density obtained from the depletion region in n-Si. The second term is the drift current density from the intrinsic layer and the third term is the drift current density from the depletion region in p-Si.

The total current density for an incident photon flux at a given wavelength is

$$J(\lambda) = J_{p,\mathrm{diff}}(\lambda) + J_{n,\mathrm{diff}}(\lambda) + J_{\mathrm{drift}}(\lambda). \tag{9}$$

Table 1: The optimum parameters used in the calculations of n-i-p solar cells with different intrinsic layer materials.

Parameters	Si	β-$FeSi_2$	$BaSi_2$
Energy gap (eV)	1.12	0.85	1.086
Relative permittivity	11.9	22.5	11.17
Diffusion coefficient (cm^2/s), D_n	35		
Diffusion coefficient (cm^2/s), D_p	12.4		
Diffusion length (μm), L_n	13.2		
Diffusion length (μm), L_p	4.9		
Surface recombination velocity (cm/s), S_n	10^4		
Surface recombination velocity (cm/s), S_p	10^4		
Intrinsic quantum efficiency, η_i	0.6		
Optical reflectivity, R	0.1		

Then the total photo current is obtained by integrating all wavelengths from 300 nm to (hc/E_g) (E_g = the energy gap of the semiconductor material). The fill-factor (FF) is defined as

$$\mathrm{FF} = \frac{V_m I_m}{V_{\mathrm{oc}} I_{\mathrm{sc}}}, \tag{10}$$

where $V_m I_m$ = the maximum power output which occurs at a point on the I-V curve, V_{oc} = the open-circuit voltage which occurs at the point with $I = 0$ on the I-V curve, and I_{sc} = the short-circuit current which occurs at the point with $V = 0$.

Finally, the conversion efficiency, η, is obtained as

$$\eta = \frac{V_{\mathrm{oc}} I_{\mathrm{sc}}}{P_{\mathrm{opt}}} \mathrm{FF}, \tag{11}$$

where P_{opt} = the incident optical power on the solar cell surface (W).

The optimum parameters used in this calculation are given in Table 1. The absorption spectrums of β-$FeSi_2$ and $BaSi_2$ are obtained by using the experiment results reported in [2], and the absorption spectrum of Si is obtained from [12].

3. Results and Discussion

The calculated p-Si/i-$\beta$$FeSi_2$/n-Si double heterojunction energy band diagram in thermal equilibrium is shown in Figure 2. The doping concentrations for both p-Si and n-Si layers are 10^{18} cm^{-3}. The thicknesses for both p-Si and n-Si layers are 1 μm and for intrinsic β-$FeSi_2$ (or $BaSi_2$) layer is 0.3 μm. The p-Si and n-Si layers have larger bandgap energy than β-$FeSi_2$ and $BaSi_2$. The wavelengths of solar radiation absorbed by the semiconductor materials are from 300 nm to (hc/E_g). Therefore, the β-$FeSi_2$ and $BaSi_2$ have wider wavelength absorption ranges than Si. The generation rate of electron-hole pairs in β-$FeSi_2$ n-i-p solar cell is shown in Figure 3 by calculating (1) and (2). At the surface of the solar cell (i.e., at $x = 0$), the generation rate of electron-hole pairs, $G_0(\lambda)$ ($s^{-1}m^{-3}$), is proportional to the absorption spectrum, $\alpha(\lambda)$ (m^{-1}). The thickness of intrinsic layer is 0.3 μm. The generation rate of electron-hole pairs, $G(x, \lambda)$, is a function of position, x, and the incident wavelength, λ. The

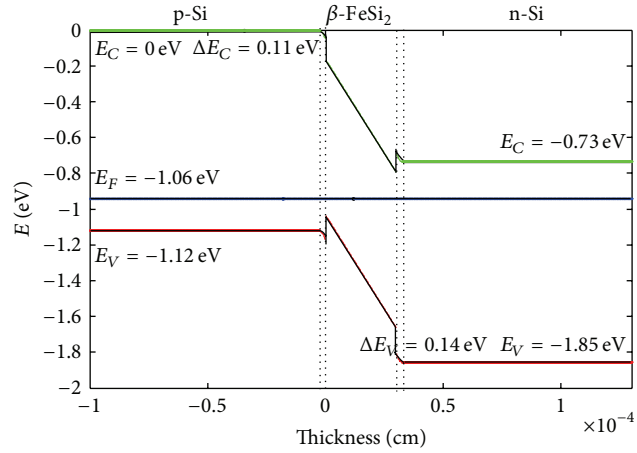

Figure 2: The equilibrium energy band diagram for p-Si/i-$\beta$$FeSi_2$/n-Si solar cell.

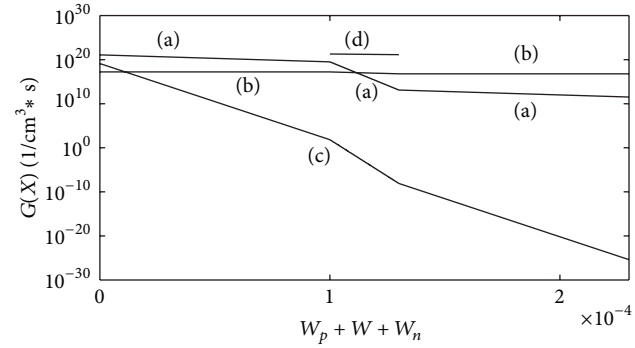

Figure 3: The generation rate as a function of position x with different wavelengths, λ, for β-$FeSi_2$ n-i-p solar cell. (a) λ = 0.405 μm, (b) λ = 1.101 μm, (c) λ = 0.305 μm, and (d) λ = 1.193 μm.

generation rate is exponentially decreased with the position x increased. There are four curves in Figure 3 corresponding to four different incident wavelengths. Note that, at incident optical wavelength λ = 1.193 μm (curve (d)), the generation rate is zero in Si regions, but in β-$FeSi_2$ region, the generation rate reaches maximum. Figure 4 shows the generation rate of electron-hole pairs in $BaSi_2$ n-i-p solar cell. Similarly, at incident optical wavelength λ = 1.086 μm (curve (d)), the generation rate is zero in Si regions, but in $BaSi_2$ region, the generation rate is maximum.

The minority carrier density distributions of β-$FeSi_2$ n-i-p solar cell with applied voltage $V_a = 0$ are shown in Figure 5 by solving (3) to (5). The doping concentrations in n-Si and p-Si regions are both equal to 10^{18} cm^{-3}. The intrinsic layer thickness is 0.4 μm. The slopes of these minority carrier density distributions at the depletion region edges determine the magnitudes of the diffusion currents (as shown in (6) and (7)). As shown in Figure 5, the maximum reverse hole diffusion current density is at wavelength λ = 0.55 μm (because the slope is maximum at this wavelength). The solar radiation is incident from n-Si to p-Si. Thus, the generation rates of electron-hole pairs in n-Si region are

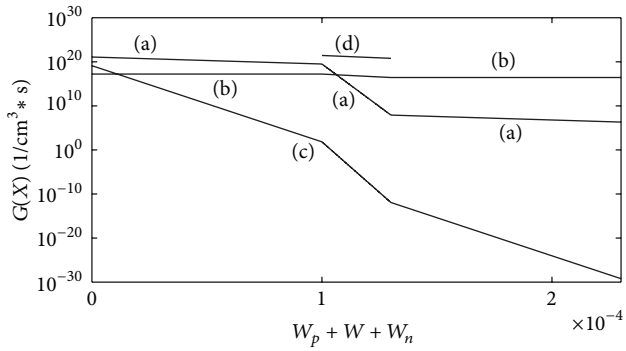

Figure 4: The generation rate as a function of position x with different wavelengths for $BaSi_2$ n-i-p solar cell. (a) $\lambda = 0.405\,\mu$m, (b) $\lambda = 1.101\,\mu$m, (c) $\lambda = 0.305\,\mu$m, and (d) $\lambda = 1.086\,\mu$m.

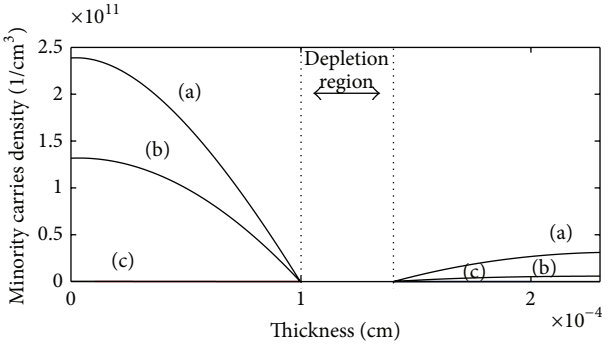

Figure 5: The minority carrier density distributions at $V_a = 0$ V for β-$FeSi_2$ solar cell with different wavelengths. (a) $\lambda = 0.455\,\mu$m, (b) $\lambda = 0.665\,\mu$m, and (c) $\lambda = 1.101\,\mu$m.

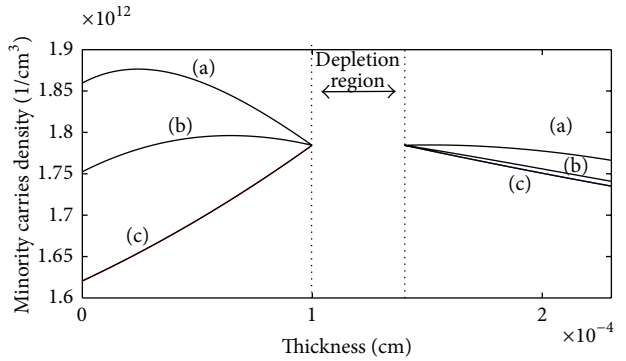

Figure 6: The minority carrier density distributions at $V_a = V_{oc} = 0.591$ V for β-$FeSi_2$ solar cell with different wavelengths. (a) $\lambda = 0.455\,\mu$m, (b) $\lambda = 0.665\,\mu$m, and (c) $\lambda = 1.101\,\mu$m.

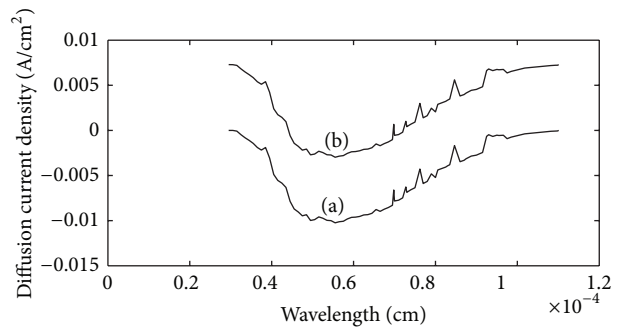

Figure 7: The calculated minority carrier diffusion current densities as a function of wavelengths for β-$FeSi_2$ solar cell. (a) $V_a = 0$ V, (b) $V_a = V_{oc} = 0.591$ V.

larger than that in p-Si region. Therefore, the minority carrier density in n-Si region is larger than that in p-Si region at all wavelengths (as shown in Figure 5). And the diffusion current density is mainly determined by the hole diffusion current density. When the applied voltage reaches the open-circuit voltage ($V_{oc} = 0.591$ V, now the total current is zero), the minority carrier density distributions of β-$FeSi_2$ solar cell are shown in Figure 6. Compared with Figure 5, the minority carrier densities are increased exponentially with applied forward-biased voltage at the edges of depletion region. And the hole diffusion current density is negative at $\lambda = 0.455\,\mu$m but is positive at $\lambda = 1.101\,\mu$m. The calculated minority carrier diffusion current densities as a function of wavelengths for β-$FeSi_2$ solar cell are shown in Figure 7 by calculating (6) and (7). When the applied voltage is zero (curve (a)), all of the minority carrier diffusion current densities are negative, and the maximum negative diffusion current density is at wavelength $\lambda = 0.55\,\mu$m. When the applied voltage reaches the open-circuit voltage, $V_{oc} = 0.591$ V (curve(b)), the minority carrier diffusion current densities are still negative at wavelengths $0.5\,\mu$m to $0.7\,\mu$m, but the magnitudes are decreased. However, at wavelengths between $0.3\,\mu$m to $0.5\,\mu$m and $0.7\,\mu$m to $1.1\,\mu$m, the minority carrier diffusion current densities become positive, and the maximum values are at $0.3\,\mu$m and $1.1\,\mu$m. The calculated drift current densities as a function of wavelengths for β-$FeSi_2$ solar cell are shown in Figure 8 by calculating (8). The drift current densities are calculated in the depletion regions. They are almost the same between $V_a = 0$ V (curve (a)) and $V_a = V_{oc} = 0.591$ V (curve (b)). The drift current densities are always negative and are almost a constant for different wavelengths.

The calculated I-V curves with different intrinsic layer materials (the intrinsic layer thickness is $0.5\,\mu$m now) are shown in Figure 9. The reverse current density of $BaSi_2$ n-i-p solar cell is larger than that of β-$FeSi_2$ and Si n-i-p solar cells. The calculated results of Figure 9 are listed in Table 2. Note that $BaSi_2$ has the maximum open-circuit current density ($|J_{sc}| = 22.93$ mA/cm^2), the maximum fill factor (FF = 82.63%), and the maximum conversion efficiency (η = 30.4%). The calculated optimum conversion efficiency of β-$FeSi_2$ n-i-p solar cells is 27.8% and that of Si n-i-p solar cell is 20.6%. $BaSi_2$ has the maximum absorption spectrum and Si has the minimum absorption spectrum. Therefore, the calculation results of conversion efficiency for different materials are consistent with their absorption spectrum. The reported [10] efficiency of amorphous Si : H (pin) solar cell is 10.1%, and that of polycrystalline Si solar cell is 20.4% which is consistent with this calculation work. Thus, the calculation results are valid in this work.

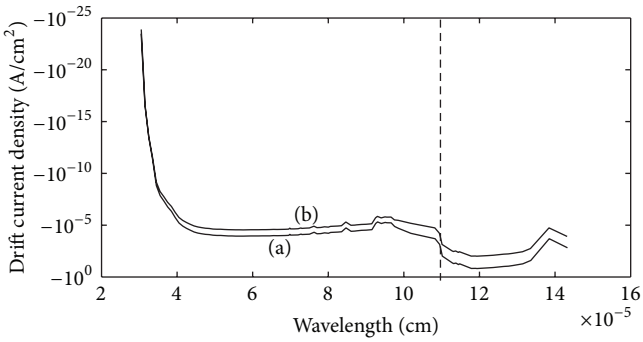

Figure 8: The calculated drift current densities as a function of wavelengths for β-$FeSi_2$ solar cell. (a) $V_a = 0$ V, (b) $V_a = V_{oc} = 0.591$ V.

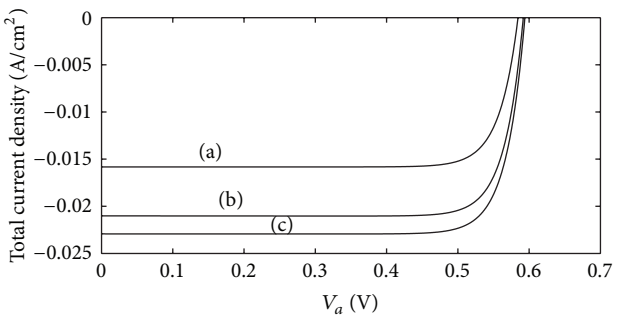

Figure 9: The calculated I-V curves of n-i-p solar cells with different intrinsic layer materials: (a) Si, (b) β-$FeSi_2$, and (c) $BaSi_2$.

Table 2: The calculated results for n-i-p solar cells with different intrinsic layer materials.

Intrinsic layer materials	V_{oc} (V)	J_{sc} (mA/cm^2)	FF (%)	η (%)
Si	0.584	15.83	82.33	20.6
β-$FeSi_2$	0.591	21.02	82.59	27.8
$BaSi_2$	0.594	22.93	82.63	30.4

4. Conclusion

The dc I-V characteristics of β-$FeSi_2$ and $BaSi_2$ n-i-p solar cells are investigated by using the analytical calculations. The distributions of minority carrier densities, the diffusion current densities of free electron and hole, and the drift current density in the depletion regions are calculated. The conversion efficiencies are obtained from the calculated I-V curves. The calculated results show that the conversion efficiency of β-$FeSi_2$ solar cell is 27.8% and that of $BaSi_2$ solar cell is 30.4%, both are larger than that of the Si n-i-p solar cell (η is 20.6% which is consistent with the reported results). These results are consistent with their absorption spectrum.

Conflict of Interests

The authors declare that there is no conflict of interests regarding the publication of this paper.

References

[1] S. P. Murarka, "Refractory silicides for integrated circuits," *Journal of Vacuum Science & Technology*, vol. 17, p. 775, 1980.

[2] D. Leong, M. Harry, K. J. Reeson, and K. P. Homewood, "A silicon/iron-disllicide light-emitting diode operating at a wavelength of 1.5 μm," *Nature*, vol. 387, no. 6634, pp. 686–688, 1997.

[3] K. Noda, Y. Terai, S. Hashimoto, K. Yoneda, and Y. Fujiwara, "Modifications of direct transition energies in β-$FeSi_2$ epitaxial films grown by molecular beam epitaxy," *Applied Physics Letters*, vol. 94, Article ID 241907, 2009.

[4] G. K. Dalapati, S. L. Liew, A. S. W. Wong, Y. Chai, S. Y. Chiam, and D. E. Chi, "Photovoltaic characteristics of p-β-$FeSi_2$(Al)/n-Si(100) heterojunction solar cells and the effects of interfacial engineering," *Applied Physics Letters*, vol. 98, Article ID 013507, 2011.

[5] Z. Lin, S. Wang, N. Otogawa et al., "A thin-film solar cell of high-quality β-$FeSi_2$/Si heterojunction prepared by sputtering," *Solar Energy Materials and Solar Cells*, vol. 90, no. 3, pp. 276–282, 2006.

[6] Y. Gao, H. W. Liu, Y. Lin, and G. Shao, "Computational design of high efficiency $FeSi_2$ thin-film solar cells," *Thin Solid Films*, vol. 519, no. 24, pp. 8490–8495, 2011.

[7] K. Morita, Y. Inomata, and T. Suemasu, "Optical and electrical properties of semiconducting $BaSi_2$ thin films on Si substrates grown by molecular beam epitaxy," *Thin Solid Films*, vol. 508, no. 1-2, pp. 363–366, 2006.

[8] D. Tsukada, Y. Matsumoto, R. Sasaki et al., "Fabrication of (111)-oriented Si layers on SiO_2 substrates by an aluminum-induced crystallization method and subsequent growth of semiconducting $BaSi_2$ layers for photovoltaic application," *Journal of Crystal Growth*, vol. 311, no. 14, pp. 3581–3586, 2009.

[9] Y. Matsumoto, D. Tsukada, R. Sasaki et al., "Epitaxial growth and photoresponse properties of $BaSi_2$ layers toward Si-based high-efficiency solar cells," *Japanese Journal of Applied Physics*, vol. 49, no. 4S, Article ID 04DP05, 2010.

[10] S. O. Kasap, *Optoelectronics and Photonics*, Pearson, 2nd edition, 2013.

[11] S. L. Chuang, *Physics of Photonic Devices*, John Wiley & Sons, New York, NY, USA, 2nd edition, 2009.

[12] A. Bosio and A. Romeo, *Thin Film Solar Cells: Current Status and Future Trends*, Nova Science Publishers, New York, NY, USA, 2011.